International Journal of Heat and Mass Transfer 103 (2016) 773–782

Contents lists available at ScienceDirect

International Journal of Heat and Mass Transfer

journal homepage: www.elsevier.com/locate/ijhmt

Thermodynamic analysis of gas flow and heat transfer in microchannels

Yangyu Guo, Moran Wang *

Key Laboratory for Thermal Science and Power Engineering of Ministry of Education, Department of Engineering Mechanics and CNMM, Tsinghua University, Beijing 100084, China

ARTICLE INFO

Article history:
Received 4 June 2016
Accepted 25 July 2016

Keywords:
Entropy generation
Second-law analysis
Microscale gas flow
Microscale heat convection
Thermodynamic optimization

ABSTRACT

Thermodynamic analysis, especially the second-law analysis, has been applied in engineering design and optimization of microscale gas flow and heat transfer. However, following the traditional approaches may lead to decreased total entropy generation in some microscale systems. The present work reveals that the second-law analysis of microscale gas flow and heat transfer should include both the classical bulk entropy generation and the interfacial one which was usually missing in the previous studies. An increase of total entropy generation will thus be obtained. Based on the kinetic theory of gases, the mathematical expression is provided for interfacial entropy generation, which shows proportional to the magnitude of boundary velocity slip and temperature jump. Analyses of two classical cases demonstrate validity of the new formalism. For a high-Kn flow and heat transfer, the increase of interfacial transport irreversibility dominates. The present work may promote understanding of thermodynamics in microscale heat and fluid transport, and throw light on thermodynamic optimization of microscale processes and systems.

1. Introductions

In recent years, with the rapid development of micro- and nanofabrication and nanotechnology [1] and micro-electromechanical systems (MEMS) [2], there are increasing interests and studies on microscale gas flow [3–7] and heat transport [8–11]. The thermodynamics at microscale has attached more and more attentions in theory, such as the non-equilibrium entropy [12–14], or in applications for optimization of thermal efficiency of microsystems. The entropy generation minimization principle [15] or so-called the second-law analysis [16], originated in classical irreversible thermodynamics (CIT) [17], has been extended from the conventional engineering field to microscale systems. Hitherto the second-law analysis of microscale gas heat convections in simple geometries (micro-channels, micro-pipes, micro-ducts, etc.) has been widely performed via either analytical approach [18–24] or numerical simulations [25–28]. All these works followed the traditional methodology: "computing the entropy generation after a resolution of velocity and temperature field distributions" based on the entropy generation formula in terms of velocity and temperature gradients [15,16]. The size effects at microscale were incorporated in obtaining the velocity and temperature distributions by solving the classical hydrodynamic equations with velocity slip and temperature jump boundary conditions. A common conclusion was made that the total entropy generation decreased with the increase of Knudsen number (Kn, defined as the ratio of mean free path to characteristic length) in microscale systems such as in the classical work [18,19].

However, the particular phenomena of velocity slip and temperature jump occur at the gas–solid interface in microscale gas flow [4]. The non-continuous velocity and temperature profiles come from the in-sufficient interactions between gas molecules and solid walls. In other words, the gas-surface interaction near the solid wall cannot reach a local equilibrium state as a fundamental hypothesis in CIT [17]. Such a non-equilibrium effect, non-doubtfully, will bring additional irreversibility and entropy generation. Actually the entropy generation in rarefied gas systems has been declared to consist of two parts [29]: one from the intermolecular interactions and the other from the gas-surface interactions, which are denoted as the bulk and the interfacial entropy generations, respectively hereafter. The study on interfacial entropy generation originated earlier in formulating fluid–solid interfacial boundary conditions in the frame of non-equilibrium thermodynamics [30,31]. The boundary conditions were obtained as bilinear phenomenological flux-force relations from the non-negative interfacial entropy generation restricted by the second law [30]. The kinetic theory foundations were also investigated rooted in linearized Boltzmann transport equation (BTE) [32–34], where both the boundary conditions and the Onsager reciprocal relations for kinetic coefficients [29,35,36] have been derived. These outstanding works laid a solid basis for interfacial boundary conditions from both thermodynamic and statistical physical perspectives. But they mainly focus on the rarefied gas transport with

* Corresponding author.
E-mail address: mrwang@tsinghua.edu.cn (M. Wang).

http://dx.doi.org/10.1016/j.ijheatmasstransfer.2016.07.093
0017-9310/

Nomenclature

$\mathbf{c}$ (c_x, c_y, c_z)	molecular velocity [m/s]
$\mathbf{u}$ (u_x)	fluid velocity [m/s]
T	thermodynamic temperature [K]
x, y, r	coordinate components [m]
Pr	Prandtl number [–]
Kn	Knudsen number [–]
Br	Brinkman number [–]
c_p	specific heat capacity at constant pressure [J/(kg·K)]
$\dot{m}$	mass flow rate [kg/s]
A_c	cross-sectional area [m^2]
R	radius of the micro-pipe [m]
H	half of the height of the micro-channel [m]
k	thermal conductivity of fluid [W/(m·K)]
P	wetting perimeter [m]
Y	dimensionless value of y [–]
q	heat flux supply [W/m^2]
A, B	combinational parameters [–]
f	molecular velocity distribution function [m^{-3}(m/s)$^{-1}$]
$\mathbf{F}$	external force on per unit mass of fluid [m/s^2]
k_B	Boltzmann constant [J/K]
p	thermodynamic pressure [Pa]
e	specific internal energy [J/kg]
s	specific entropy or specularity parameter of wall [J/(K·kg)] or [–]
$\mathbf{J}^s$	entropy flux [W/(K·m^2)]
S_{gen}	entropy generation rate [W/K]

Greek symbols

λ	molecular mean free path [m]
μ	dynamic viscosity of fluid [kg/(m·s)]
ρ	mass density of fluid [kg/m^3]
γ	specific heat ratio [–]
τ	molecular relaxation time [s]
θ	dimensionless temperature [–]
η	dimensionless value of r [–]
σ	entropy generation rate per unit volume [W/(K·m^3)]
Φ_q	dissipation function [s^{-2}]
Φ, ϕ	deviational part of velocity distribution function [–]
α, β	dummy index [–]

Subscripts

s	variables of gas at the wall
w	variables of the wall
m	mean value of variables
1	parameters of micro-pipe
2	parameters of micro-channel
eq	equilibrium state
b	bulk region
i	interface region

Acronyms

CIT	classical irreversible thermodynamics
BTE	Boltzmann transport equation

a finite Kn resulting from enhanced mean free path. Theoretical foundation of the entropy generation is seldom explored in microscale gas flow and heat transport, where the reduced system size contributes to the finite Kn. It will be shown that the interfacial entropy generation obtained in rarefied gas transport is not available directly to analysis of microscale gas flows due to a finite portion of Knudsen layer (a thin layer with a thickness about one mean free path near the wall) across the microchannel. On the other hand, the interfacial entropy generation has never been incorporated into the second-law analysis of microscale gas heat convections in the previous work [18–28], to the authors' best knowledge. With the miniaturization of system and increase of Kn, the entropy generation at the interface may become comparable to or even dominant over that in the bulk region. The thermodynamic performance of microscale system will thus be inadequately or erroneously evaluated when neglecting the interfacial irreversibility. It will be shown that the total entropy generation may increase with increasing Kn when both the bulk and interfacial entropy generations are counted.

Therefore, the present work aims at a systematic second-law analysis of microscale gas flow and heat transport with special attention on the role of interfacial entropy generation. Two classical cases are taken for demonstration: heat convections in micro-pipe [37] and in micro-channel [38]. The remainder of this article is organized as: in Section 2, the mathematical expressions of bulk and interfacial entropy generation are derived respectively in the frame of CIT and gas kinetic theory, as the theoretical foundation of second-law analysis. In Section 3, the analytical solutions and then the specific entropy generation formulations of heat convections in micro-pipe and micro-channel are presented. In Section 4, we provide the results of second-law analysis of the two cases of microscale heat convection in Section 3, with the role of interfacial irreversibility to be illustrated and discussed. Concluding remarks are finally made in Section 5.

2. Theoretical foundation of second-law analysis

The theoretical evaluation of thermodynamic irreversibility in microscale gas flow is intimately related to its hydrodynamic modeling, as is shown in Fig. 1. The microscale gas flow within the slip regime ($0.001 \leqslant Kn \leqslant 0.1$) is considered throughout the present work, modeled by the Navier–Stokes equation (or Fourier's law) with a velocity slip (or temperature jump) boundary condition [4]. Although in principle the gas behaviors within the Knudsen layer should be described through a solution of BTE, the present modeling has been proved to yield sufficiently accurate results within the slip regime [4,7]. Accordingly, the total entropy generation includes twofold shown in Fig. 1(b): the bulk part in the microchannel due to the fluid flow (or heat transport) and the interfacial part at the wall induced by velocity slip (or temperature jump). The interfacial entropy generation has been calculated for rarefied gas transport based on kinetic theory of gases, as the difference between the entropy fluxes at the gas side and the solid one [32–34]. The velocity distribution function of gases obtained by the Chapman–Enskog solution to BTE in the bulk region (outside the Knudsen layer) was used to evaluate the entropy flux at the gas side. From the authors' perspective, the obtained entropy generation is actually that within the Knudsen layer, as shown in Fig. 1(c). As the Knudsen layer is modeled approximately by continuum equation, the entropy generation within this layer has been accounted in the bulk part, as indicated in Fig. 1(b). Direct application of previous interfacial entropy generation here will duplicate the entropy generation in the Knudsen layer. Thus in the present work, the interfacial entropy generation is derived as the difference between entropy flux of gas at the wall and entropy flux in the solid wall. The former one is evaluated based on the velocity distribution functions of incident gases (f^-) and reflecting gases (f^+) at the wall, which are related by the Maxwell gas-surface interaction model, as shown in Fig. 1(d). The obtained interfacial entropy

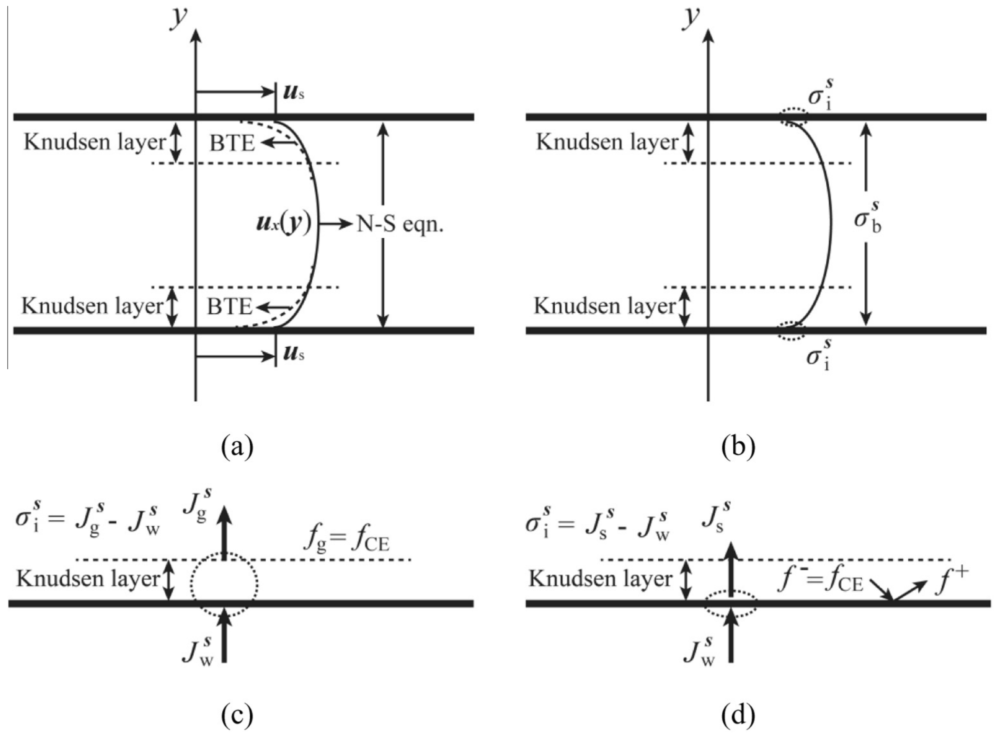

Fig. 1. Hydrodynamic modeling and thermodynamic irreversibility of microchannel gas flow in slip regime: (a) Modeling by Navier–Stokes equation with slip boundary condition, with also a comparison to the BTE solution in Knudsen layer (dashed line); (b) The total entropy generation including the bulk part σ_b^s and interfacial part σ_i^s; (c) Kinetic theory foundation of σ_i^s in previous work, as the difference between entropy flux of gases in the bulk region near the wall (J_g^s) and entropy flux in the solid wall (J_w^s), with J_g^s computed based on the Chapman–Enskog distribution function outside the Knudsen layer $f_g = f_{CE}$; (d) Kinetic theory foundation of σ_i^s in the present work, as the difference between entropy flux of gas at the wall (J_s^s) and entropy flux in the solid wall (J_w^s), with J_s^s computed based on the distribution functions of incident gas (f^-) and reflecting gas (f^+) which are related by the Maxwell gas-surface interaction model.

generation in the present work is lower than that for rarefied gas transport. The detailed derivation of bulk and interfacial entropy generations is given below in the frame of CIT and kinetic theory of gases separately.

2.1. Bulk entropy generation

The entropy generation in the bulk region is derived in the frame of CIT. The balance equations of mass and energy for heat and fluid flow are [39]:

$$\begin{aligned} &\frac{d\rho}{dt} + \rho\nabla\cdot\mathbf{u} = 0 \\ &\rho\frac{de}{dt} = -\nabla\cdot\mathbf{q} - \mathbf{P}:\nabla\mathbf{u} \end{aligned}, \tag{1}$$

with e the specific internal energy of fluid, $\mathbf{q}$ and $\mathbf{P}$ the heat flux vector and pressure tensor, governed by the Fourier's law and Newton's shear law respectively [39]:

$$\begin{aligned} &\mathbf{q} = -k\nabla T \\ &\mathbf{P} = p\mathbf{I} - \mu\left[\nabla\mathbf{u} + (\nabla\mathbf{u})^{\mathrm{T}}\right] + \frac{2}{3}\mu(\nabla\cdot\mathbf{u})\mathbf{I} \end{aligned}, \tag{2}$$

with $\mathbf{I}$ the unit tensor, the superscript 'T' in roman denoting the transpose of a tensor, distinguished from the normal T in italics denoting the temperature. Here the bulk viscosity of fluid has not been considered. The fundamental relation in CIT is the Gibbs equation [17]:

$$T\frac{ds}{dt} = \frac{de}{dt} - \frac{p}{\rho^2}\frac{d\rho}{dt}. \tag{3}$$

Substitution of Eqs. (1) and (2) into Eq. (3), with an identification to the entropy balance equation [17]:

$$\rho\frac{ds}{dt} = -\nabla\cdot\mathbf{J}^s + \sigma_b^s, \tag{4}$$

gives rise to the expressions of entropy flux and entropy generation respectively:

$$\mathbf{J}^s = \mathbf{q}/T, \tag{5}$$

$$\sigma_b^s = \frac{k}{T^2}(\nabla T)^2 + \frac{\mu}{T}\left[\nabla\mathbf{u} + (\nabla\mathbf{u})^{\mathrm{T}}\right] : \nabla\mathbf{u} - \frac{2}{3}\frac{\mu}{T}(\nabla\cdot\mathbf{u})^2. \tag{6}$$

For an incompressible flow ($\nabla\cdot\mathbf{u} = 0$) considered in the present work, the bulk entropy generation Eq. (6) reduces to:

$$\sigma_b^s = \frac{k}{T^2}(\nabla T)^2 + \frac{\mu}{T}\left[\nabla\mathbf{u} + (\nabla\mathbf{u})^{\mathrm{T}}\right] : \nabla\mathbf{u}. \tag{7}$$

Eq. (7) evaluates the thermodynamic irreversibility induced by bulk heat conduction and viscous flow.

2.2. Interfacial entropy generation

The interfacial entropy generations induced by the velocity slip and temperature jump in microscale gas flow and heat transport are derived based on the kinetic theory of gases. For mathematical simplicity and clear physical interpretation, the coupling effect is assumed negligible between fluid flow and heat conduction, as to be separately discussed below in Sections 2.2.1 and 2.2.2, shown in Fig. 2(a) and (b). The assumption of negligible coupling between gas flow and heat conduction may be acceptable in the slip regime where the non-equilibrium effect is moderate.

In the gas kinetic theory, the transport process is described by BTE [40]:

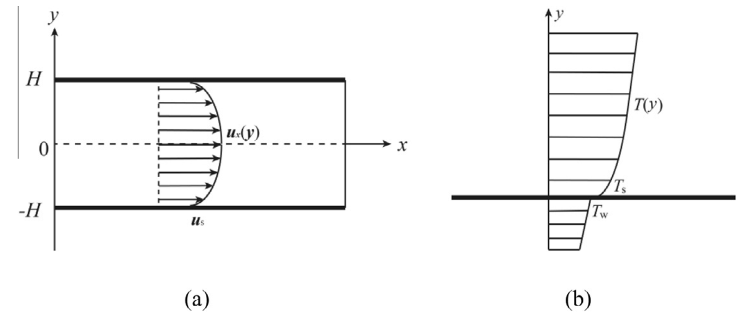

Fig. 2. Derivation of interfacial entropy generation in microscale gas flow and heat transport: (a) isothermal microscale gas flow with velocity slip; (b) microscale gas conduction with temperature jump. Steady states are considered for both cases.

$$\frac{\partial f}{\partial t}+\mathbf{c}\cdot\frac{\partial f}{\partial \mathbf{x}}+\mathbf{F}\cdot\frac{\partial f}{\partial \mathbf{c}}=C(f), \tag{8}$$

where $f=f(\mathbf{x},\mathbf{c},t)$ is the velocity distribution function, with $f\mathrm{d}\mathbf{x}\mathrm{d}\mathbf{c}$ denoting the probabilistic number of gas molecules within spatial interval $(\mathbf{x},\mathbf{x}+\mathrm{d}\mathbf{x})$ and molecular velocity interval $(\mathbf{c},\mathbf{c}+\mathrm{d}\mathbf{c})$, and $\mathbf{F}$ is the external force on per unit mass of gases. $C(f)$ is the molecular collision term, which is extremely complicated and usually assumed the BGK relaxation approximation [41]. Thus Eq. (8) without external force reduces to:

$$\frac{\partial f}{\partial t}+\mathbf{c}\cdot\frac{\partial f}{\partial \mathbf{x}}=-\frac{f-f_{\mathrm{eq}}}{\tau}, \tag{9}$$

with τ denoting the molecular relaxation time, the equilibrium distribution function f_{eq} being the local Maxwell–Boltzmann distribution [40]:

$$f_{\mathrm{eq}}=\frac{\rho}{m}\left(\frac{m}{2\pi k_{\mathrm{B}}T}\right)^{3/2}\exp\left[-\frac{m(c_\alpha-u_\alpha)^2}{2k_{\mathrm{B}}T}\right], \tag{10}$$

where k_{B} is the Boltzmann constant. Hereafter the Einstein's summation convention [39] is applied for elegance. Through a Chapman–Enskog expansion of f around f_{eq} within zero$^{\mathrm{th}}$ order, first order and higher order, different hydrodynamic equations are recovered respectively: Euler equation, Navier–Stokes equation and Burnett or super-Burnett equation [42]. In the present work, as the bulk fluid flow is described by the Navier–Stokes equations, the first-order expansion solution of Eq. (9) is adopted for further analysis [43]:

$$f=f_{\mathrm{eq}}-\left[\begin{array}{l}\frac{m^2f_{\mathrm{eq}}}{\rho(k_{\mathrm{B}}T)^2}(c_\alpha-u_\alpha)(c_\beta-u_\beta)\mu\frac{\partial u_\alpha}{\partial x_\beta}-\frac{m^2f_{\mathrm{eq}}}{3\rho(k_{\mathrm{B}}T)^2}(c_\alpha-u_\alpha)(c_\alpha-u_\alpha)\mu\frac{\partial u_\beta}{\partial x_\beta}\\-\frac{m^2f_{\mathrm{eq}}}{\rho(k_{\mathrm{B}}T)^2}(c_\alpha-u_\alpha)k\frac{\partial T}{\partial x_\alpha}+\frac{m^3f_{\mathrm{eq}}}{5\rho(k_{\mathrm{B}}T)^3}(c_\alpha-u_\alpha)(c_\alpha-u_\alpha)(c_\beta-u_\beta)k\frac{\partial T}{\partial x_\beta}\end{array}\right]. \tag{11}$$

The entropy balance equation Eq. (4) can be derived from the BTE Eq. (9) by multiplying '$-k_{\mathrm{B}}\ln f$' on both sides and integrating over the whole molecular velocity space [9]:

$$\frac{\partial}{\partial t}\left(-k_{\mathrm{B}}\int f\ln f\mathrm{d}\mathbf{c}\right)+\frac{\partial}{\partial \mathbf{x}}\cdot\left(-k_{\mathrm{B}}\int \mathbf{c}f\ln f\mathrm{d}\mathbf{c}\right)=-k_{\mathrm{B}}\int(1+\ln f)C(f)\ \mathrm{d}\mathbf{c}. \tag{12}$$

Therefore, the kinetic definitions of entropy density and entropy flux are obtained as:

$$\rho s=-k_{\mathrm{B}}\int f\ln f\mathrm{d}\mathbf{c}$$
$$\mathbf{J}^s=-k_{\mathrm{B}}\int(\mathbf{c}-\mathbf{u})f\ln f\mathrm{d}\mathbf{c}. \tag{13}$$

2.2.1. Interfacial entropy generation of velocity slip

For the fully-developed micro-channel isothermal gas flow shown in Fig. 2(a), the gas flow near the lower wall is taken to calculate the interfacial entropy generation. From Eq. (11), the distribution function of gases near the wall reduces to:

$$f^-=f_{\mathrm{eq}}^-\left[1-\frac{m^2}{\rho(k_{\mathrm{B}}T)^2}(c_x-u_{\mathrm{s}})c_y\mu\left(\frac{\partial u_x}{\partial y}\right)_{\mathrm{s}}\right], \tag{14}$$

where u_{s} is the gas slip speed at the wall and the local equilibrium distribution function becomes:

$$f_{\mathrm{eq}}^-=\frac{\rho}{m}\left(\frac{m}{2\pi k_{\mathrm{B}}T}\right)^{3/2}\exp\left[-\frac{(c_x-u_{\mathrm{s}})^2+c_y^2+c_z^2}{2k_{\mathrm{B}}T/m}\right]. \tag{15}$$

The main idea to derive the interfacial entropy generation has been proposed as the difference between the entropy fluxes at the gas side (J_{g}^s) and at the solid side (J_{w}^s) [29]:

$$\sigma_{\mathrm{i}}^s=J_{\mathrm{g}}^s-J_{\mathrm{w}}^s, \tag{16}$$

where $J_{\mathrm{w}}^s=q_{\mathrm{n}}/T$, with q_{n} the normal heat flux at the solid side and assumed equal to the normal heat flux at the gas side [34]. For the isothermal gas flow ($q_{\mathrm{n}}=0$), Eq. (16) reduces to [29,44]:

$$\sigma_{\mathrm{i}}^s=J_{\mathrm{g}}^s=-k_{\mathrm{B}}\int c_yf^-\ln f^-\mathrm{d}\mathbf{c}. \tag{17}$$

The distribution function of gases can be rewritten as $f^-=f_0(1+\Phi)$, with the global Maxwell–Boltzmann distribution $f_0=\frac{\rho}{m}\left(\frac{m}{2\pi k_{\mathrm{B}}T}\right)^{3/2}\exp\left[-\frac{m\mathbf{c}^2}{2k_{\mathrm{B}}T}\right]$. After some mathematic operations, the interfacial entropy generation Eq. (17) becomes [32–34]:

$$\sigma_{\mathrm{i}}^s=-\frac{1}{2}k_{\mathrm{B}}\int c_yf_0\Phi^2\ \ \mathrm{d}\mathbf{c}. \tag{18}$$

In this work, according to the analysis at the beginning of Section 2, the interfacial entropy generation is instead derived from $\sigma_{\mathrm{i}}^s=J_{\mathrm{s}}^s-J_{\mathrm{w}}^s=J_{\mathrm{s}}^s$ with J_{s}^s the entropy flux of gases at the wall:

$$\sigma_{\mathrm{i}}^s=-k_{\mathrm{B}}\int c_yf_{\mathrm{s}}\ln f_{\mathrm{s}}\mathrm{d}\mathbf{c}. \tag{19}$$

In Eq. (19), the distribution function of gases at the wall is:

$$f_{\mathrm{s}}=\begin{cases}f^-, & \text{for } c_y<0\\ f^+, & \text{for } c_y>0\end{cases}, \tag{20}$$

where the distribution function of reflecting gases f^+ is related to that of incident gases f^- through the gas-surface interaction model. The most common Maxwell model [44] is used here: the gas molecules collide with the wall, and experience diffuse or specular scatterings, the portion of them given by $(1-s)$ and s respectively.

Thus the distribution function of reflecting gases is formulated as [44]:

$$f^{+} = sf^{-}(c_x, -c_y) + (1-s)f_0(T_w). \tag{21}$$

Substituting Eqs. (20) and (21) into Eq. (19), we get the full expression of interfacial entropy generation:

$$\begin{aligned}\sigma_i^s = & -k_B\Bigg[\int_{-\infty}^{\infty}\int_{-\infty}^{0}\int_{-\infty}^{\infty} c_y f_0(1+\Phi)\ln[f_0(1+\Phi)]\, dc_x dc_y dc_z \\ & - \int_{-\infty}^{\infty}\int_{-\infty}^{0}\int_{-\infty}^{\infty} c_y f_0(1+s\Phi)\ln[f_0(1+s\Phi)]\, dc_x dc_y dc_z\Bigg]. \end{aligned} \tag{22}$$

The integration in Eq. (22) is too complicated for a general case (arbitrary value of s). The fully diffuse wall ($s = 0$) is considered throughout the present work, such that Eq. (22) reduces to:

$$\begin{aligned}\sigma_i^s = & -k_B\Bigg[\int_{-\infty}^{\infty}\int_{-\infty}^{0}\int_{-\infty}^{\infty} c_y f^{-}\ln f^{-}\, dc_x dc_y dc_z \\ & - \int_{-\infty}^{\infty}\int_{-\infty}^{0}\int_{-\infty}^{\infty} c_y f_0 \ln f_0\, dc_x dc_y dc_z\Bigg]. \end{aligned} \tag{23}$$

Similar to the analysis from Eq. (17) to Eq. (18), the following approximation is made (with $f^{-} = f_{eq}^{-}(1+\phi)$):

$$f^{-}\ln f^{-} \approx f_{eq}^{-}\ln f_{eq}^{-} + (1+\ln f_{eq}^{-})f_{eq}^{-}\phi + \frac{1}{2}f_{eq}^{-}\phi^2. \tag{24}$$

Substituting Eq. (24) into Eq. (23) and integrating over molecular velocity space, we obtain the explicit expression of interfacial entropy generation:

$$\sigma_i^s = \frac{\mu}{\pi T}\lambda\left[\left(\frac{\partial u_x}{\partial y}\right)_s\right]^2, \tag{25}$$

where the molecular mean free path λ has been related to the dynamic viscosity μ through $\mu = \frac{1}{2}\rho\bar{c}\lambda = \rho\lambda\sqrt{\frac{2k_BT}{\pi m}}$ [40]. With the expression of slip speed in the Maxwell model: $u_s = \lambda\left(\frac{\partial u_x}{\partial y}\right)_s$ [4], Eq. (25) is slightly reformulated as:

$$\sigma_i^s = \frac{\mu}{\pi T}u_s\left(\frac{\partial u_x}{\partial y}\right)_s. \tag{26}$$

Eq. (26) implies that the interfacial entropy generation is proportional to the gas slip speed (or velocity gradient) at the wall. For gas flows in the continuum regime, the slip speed is negligibly small, with a nearly vanishing σ_i^s. It is thus reasonable to neglect the entropy generation at the gas–solid interface and merely consider that in the bulk region, as in the traditional second-law analysis [15,16]. However, for gas flows in the slip regime where appreciable slip speed exists, Eq. (26) gives a finite value of σ_i^s. The interfacial entropy generation is no longer negligible, but may become comparable to or even dominant over that in the bulk region, as to be demonstrated below.

The deviation part (of distribution function) ϕ in Eq. (24) rather than Φ in Eq. (18) is used in present work, since it makes the analytical integration in Eq. (23) much simpler. The former is a perturbation from the local equilibrium distribution f_{eq}^{-} (Eq.(15)) whereas the latter is a perturbation from the global equilibrium distribution f_0. They are related through the identity $f^{-} = f_{eq}^{-}(1+\phi) = f_0(1+\Phi)$ and a linearization of f_{eq}^{-} around f_0 [33,34]:

$$\Phi = \frac{\delta p(0)}{p} + \frac{\delta T(0)}{T}\left(\frac{mc_\alpha^2}{2k_BT} - \frac{5}{2}\right) + \frac{mc_\alpha u_\alpha(0)}{k_BT} + \phi, \tag{27}$$

where the temperature and pressure jumps $\delta T(0)$, $\delta p(0)$ are perturbations from the global equilibrium state at the gas–solid interface and vanish for the present isothermal flow. In this way, Eq. (27) reduces to:

$$\Phi = \frac{mc_x u_s}{k_BT} + \phi. \tag{28}$$

Substitution of Eq. (28) into Eq. (18) produces the interfacial entropy generation obtained in the previous work [33,34]:

$$\sigma_i^s = \frac{\mu}{T}u_s\left(\frac{\partial u_x}{\partial y}\right)_s. \tag{29}$$

The interfacial entropy generation Eq. (26) derived in the present work is lower than the previous one in Eq. (29), although they have the same mathematical form. The reason has been elucidated in Fig. 1, where Eq. (29) signifies actually the entropy generation within the Knudsen layer while Eq. (26) is the entropy generation at the interface needed for second-law analysis. One should note that the Knudsen layer correction is sometimes taken into account for the distribution function of gases near the wall [33], which will slightly improve the accuracy through a sacrifice of simplicity. Since an accurate analytical modeling of Knudsen layer remains still an open question [7,42], the correction is not considered for the moment.

2.2.2. Interfacial entropy generation of temperature jump

For the microscale gas heat conduction shown in Fig. 2 (b), the gas conduction near the wall is considered. From Eq. (11), the distribution function of gases near the wall reduces to:

$$f^{-} = f_{eq}^{-}\left\{1 + \frac{k}{\rho(k_BT_s/m)^2}\left(\frac{\partial T}{\partial y}\right)_s c_y\left[1 - \frac{(c_x^2+c_y^2+c_z^2)}{5k_BT_s/m}\right]\right\}, \tag{30}$$

with the equilibrium distribution function:

$$f_{eq}^{-} = \frac{\rho}{m}\left(\frac{m}{2\pi k_BT_s}\right)^{3/2}\exp\left[-\frac{c_x^2+c_y^2+c_z^2}{2k_BT_s/m}\right]. \tag{31}$$

In principle, the interfacial entropy generation of temperature jump could be derived through similar procedures for that of velocity slip in Section 2.2.1. However, it is nontrivial to obtain the entropy flux in the non-equilibrium solid side near the interface

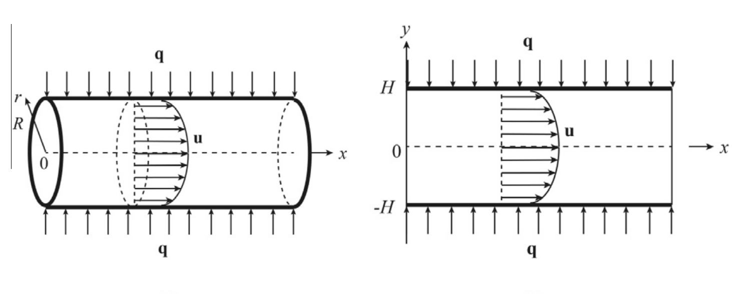

Fig. 3. Schematic of fully-developed microscale gas heat convections: (a) in circular micro-pipe; (b) in parallel micro-channel. For both cases, isoflux walls are considered.

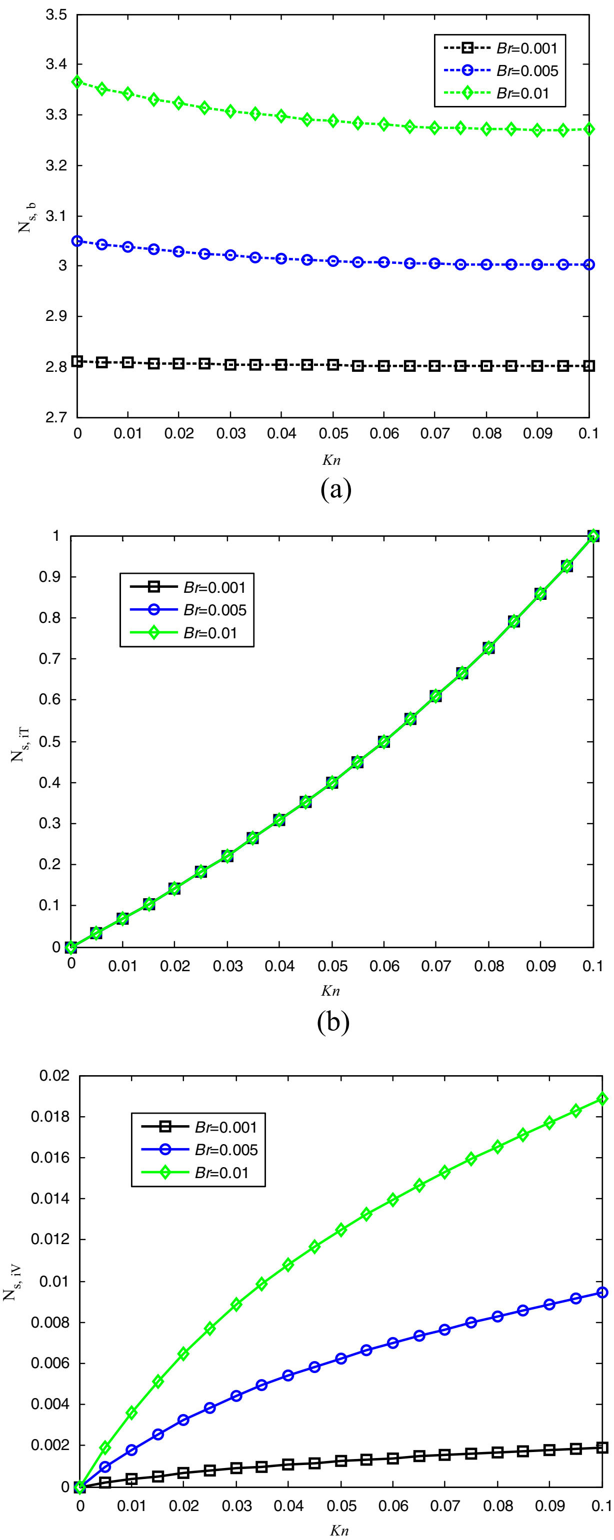

Fig. 4. Entropy generation number versus *Kn* for heat convection in micro-pipe: (a) bulk entropy generation number; (b) interfacial entropy generation number induced by temperature jump; (c) interfacial entropy generation number induced by velocity slip. Pr = 0.7, $\gamma = 1.4$, $\theta_w = 1$. Three different *Br*s are considered: *Br* = 0.001 (black square-line), *Br* = 0.005 (blue circle-line), *Br* = 0.01(green diamond-line). The dashed lines with symbols represent the bulk entropy generation number whereas the solid lines with symbols represent the interfacial entropy generation numbers. (For interpretation of the references to color in this figure legend, the reader is referred to the web version of this article.)

because of the distinction between kinetic theories of solids and gases. Therefore the interfacial entropy generation is approximately estimated as a difference between entropy fluxes at the gas side and at the solid side assuming the classical form (cf. Eq. (5)):

$$\sigma_i^s = J_w^s - J_s^s = \frac{q_n}{T_w} - \frac{q_n}{T_s}. \tag{32}$$

A deeper microscopic exploration is still needed of the interfacial irreversibility of heat conduction across the gas–solid interface, as a current important topic.

To sum up, the expressions of interfacial entropy generations induced by velocity slip and temperature jump are derived as Eqs. (26) and (32) respectively. Their dimension is slightly different from the bulk entropy generation Eq. (7): the former denotes entropy generated in unit interfacial area while the latter denotes the entropy generated in unit volume. The present Section 2 provides a theoretical ground for the second-law analysis of the two cases of microscale heat convection introduced in next section.

3. Physical and mathematical models

The microscale heat convection in parallel micro-channel and circular micro-pipe in the near-continuum and slip regimes are taken for a demonstration of second-law analysis in this section. The analytical solutions of the two classical cases shown in Fig. 3 are obtained as a first step, after which the specific formulations of entropy generations are provided respectively. The following assumptions are made [19,37,38]: (***i***) Steady-state incompressible laminar gas flow; (***ii***) Both hydrodynamically and thermally fully-developed; (***iii***) Neglected axial heat conduction; (***iv***) Constant properties. The analytical solutions of these two problems have been indeed obtained in the classical work [37,38]. But slightly different trains of thought in the solution such as the used dimensionless parameters will lead to different expressions of the final result, as shown in Ref. [19]. Therefore, the present work follows the general lines in analytically solving the conventional heat convection in any classical heat transfer textbook [45], with the microscale effect taken into account through the boundary conditions.

Microscale gas flow in the slip regime can be modeled by the Navier–Stokes equations supplemented with non-continuous boundary conditions [4]. The first-order velocity slip and temperature jump boundary conditions at the fully-diffuse wall are respectively [4]:

$$u_s - u_w = \lambda \left(\frac{\partial u}{\partial y}\right)_s, \tag{33}$$

$$T_s - T_w = \frac{2\gamma}{\gamma + 1} \frac{\lambda}{\mathrm{Pr}} \left(\frac{\partial T}{\partial y}\right)_s, \tag{34}$$

with γ the specific heat ratio and Pr the Prandtl number. Zero wall velocity ($u_w = 0$) is considered.

The rigorous condition for thermally fully-developed heat convection is [45]:

$$\frac{\partial}{\partial x}\left[\frac{T_s(x) - T(y,x)}{T_s(x) - T_m(x)}\right] = 0, \tag{35}$$

with x denoting the axial coordinate of the channel or pipe, y (or r) the normal (or radial) coordinate. The cross-sectional mean temperature is defined based on the energy flow rate [19,45]:

$$T_m = \frac{\int_{A_c} \rho u c_p T \mathrm{d}A}{\dot{m} c_p}, \tag{36}$$

where the mass flow rate of gas is $\dot{m} = \rho u_m A_c$, with A_c and u_m being respectively the cross-sectional area and mass mean velocity. For an isoflux-wall case considered here, Eq. (35) reduces to [45]:

$$\frac{\partial T}{\partial x} = \frac{\mathrm{d}T_s}{\mathrm{d}x} = \frac{\mathrm{d}T_m}{\mathrm{d}x}. \tag{37}$$

3.1. Heat convection in micro-pipe

The velocity distribution is obtained through a solution of Navier–Stokes equation with the first-order slip boundary condition Eq. (33) [4]:

$$u = 2u_m \frac{1 + 4Kn - (r/R)^2}{1 + 8Kn}, \tag{38}$$

with the Knudsen number defined as $Kn = \lambda/2R$. The temperature differential equation including the viscous dissipation heat, becomes [45]:

$$\rho c_p u \frac{\partial T}{\partial x} = \frac{k}{r}\frac{\partial}{\partial r}\left(r\frac{\partial T}{\partial r}\right) + \mu\,\Phi_q, \tag{39}$$

where Φ_q is the dissipation function [39], and in the present case reduces to:

$$\Phi_q = \left(\frac{\partial u}{\partial r}\right)^2. \tag{40}$$

The energy balance equation for a specific cross section of the pipe is [19]:

$$\frac{\mathrm{d}T_m}{\mathrm{d}x} = \frac{1}{\dot{m}c_p}\left(qP + \int_{A_c} \mu\,\Phi_q\,\mathrm{d}A\right), \tag{41}$$

with the total mass flow rate of gas through the cross section $\dot{m} = \rho u_m \pi R^2$, the wetting perimeter $P = 2\pi R$, and the differential area element $\mathrm{d}A = 2\pi r\mathrm{d}r$. Substitution of Eqs. (37), (38), (40) and (41) into Eq. (39) gives rise to a dimensionless temperature differential equation:

$$\frac{\mathrm{d}}{\mathrm{d}\eta}\left(\eta\frac{\mathrm{d}\theta}{\mathrm{d}\eta}\right) = 4\eta\frac{1 + 4Kn - \eta^2}{1 + 8Kn}\left[1 + \frac{8Br}{(1 + 8Kn)^2}\right] - \frac{32Br\eta^3}{(1 + 8Kn)^2}, \tag{42}$$

where the dimensionless temperature and coordinate are introduced respectively as: $\theta = kT/qR$, $\eta = r/R$. The Brinkman number is defined as the ratio of viscous dissipation heat to the external heat supply [37]: $Br = \mu u_m^2/2Rq$.

The dimensionless forms of symmetrical boundary conditions and temperature jump boundary conditions for Eq. (42) are:

$$\begin{aligned} &\eta = 0, \quad \frac{\mathrm{d}\theta}{\mathrm{d}\eta} = 0 \\ &\eta = 1, \quad \theta = \theta_s = \theta_w - \frac{4\gamma}{\gamma + 1}\frac{Kn}{\mathrm{Pr}} \end{aligned}. \tag{43}$$

Solution of Eq. (42) with the boundary conditions Eq. (43) results in the analytical radial temperature distribution:

$$\theta = \theta_w - \frac{4\gamma}{\gamma + 1}\frac{Kn}{\mathrm{Pr}} + \mathrm{B}_1(\eta^2 - 1) + \mathrm{A}_1(1 - \eta^4), \tag{44}$$

where the combinational parameters A_1, B_1 are defined as:

$$\begin{aligned} \mathrm{A}_1 &\equiv \left[1 + \frac{16Br(1 + 4Kn)}{(1 + 8Kn)^2}\right]\frac{1}{4(1 + 8Kn)} \\ \mathrm{B}_1 &\equiv \left[1 + \frac{8Br}{(1 + 8Kn)^2}\right]\frac{1 + 4Kn}{1 + 8Kn} \end{aligned}. \tag{45}$$

It is trivial to validate that the present analytical solutions of velocity and temperature distributions are consistent with those in previous work [19,37]. Therefore, the velocity and temperature fields are reliable for an accurate evaluation of entropy generation in the next step.

The source of entropy generation in microscale heat convection contains four parts: (***i***) viscous flow and (***ii***) heat conduction in the bulk region; (***iii***) velocity slip and (***iv***) temperature jump at the gas–solid interface. Thus the total entropy generation is formulated as:

$$S_{gen} = S_{gen,\,H} + S_{gen,\,F} + S_{gen,V} + S_{gen,T}, \tag{46}$$

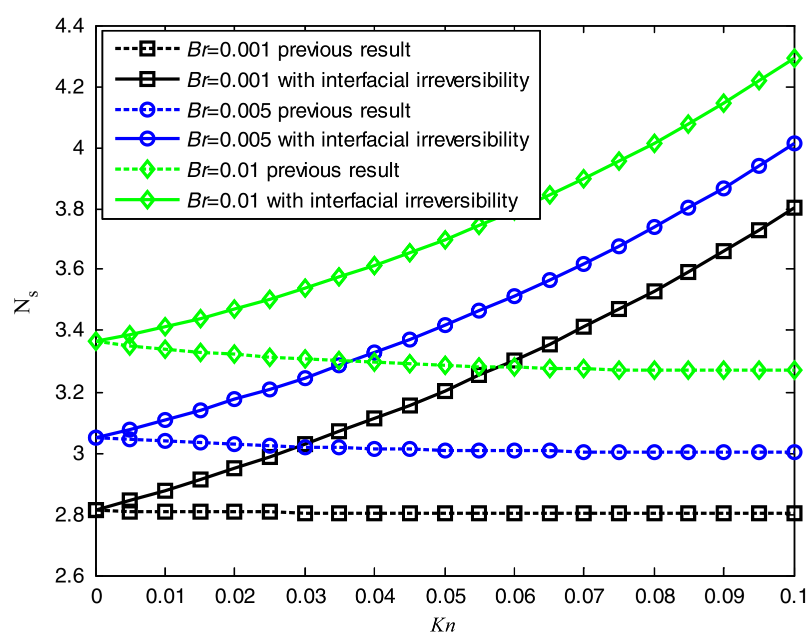

Fig. 5. Total entropy generation number of heat convection in micro-pipe versus *Kn*. Pr = 0.7, γ = 1.4, θ_w = 1. Three different *Br*s are considered: *Br* = 0.001 (black square-line), *Br* = 0.005 (blue circle-line), *Br* = 0.01(green diamond-line). The solid lines with symbols represent the present second-law analysis counting both the bulk and interfacial entropy generations, while the dashed lines with symbols represent the previous second-law analysis counting only the bulk entropy generation. (For interpretation of the references to color in this figure legend, the reader is referred to the web version of this article.)

with the subscripts 'H', 'F', 'V', 'T' represent 'heat conduction', 'fluid flow', 'velocity slip' and 'temperature jump' respectively. Taking a volume element $dV = A_c dx$ across the pipe at $(x, x + dx)$, each part of the entropy generation is computed as below:

$$S_{\mathrm{gen,H}} = \int_V \sigma_{\mathrm{H}}^s dV = \int_V \frac{k}{T^2}(\nabla T)^2 dV = dx \int_{A_c} \frac{k}{T^2}\left(\frac{\partial T}{\partial r}\right)^2 dA, \tag{47}$$

$$S_{\mathrm{gen,F}} = \int_V \sigma_{\mathrm{F}}^s dV = \int_V \frac{\mu}{T}\left(\frac{du}{dr}\right)^2 dV = dx \int_{A_c} \frac{\mu}{T}\left(\frac{du}{dr}\right)^2 dA, \tag{48}$$

$$S_{\mathrm{gen,V}} = \int_\Sigma \sigma_{\mathrm{V}}^s d\Sigma = \int_\Sigma \frac{\mu}{\pi T_s} u_s \left(\frac{du}{dr}\right)_s d\Sigma = P dx \frac{\mu}{\pi T_s} u_s \left(\frac{du}{dr}\right)_s, \tag{49}$$

$$S_{\mathrm{gen,T}} = \int_\Sigma \sigma_{\mathrm{T}}^s d\Sigma = \int_\Sigma q\left(\frac{1}{T_s} - \frac{1}{T_w}\right) d\Sigma = P dx q\left(\frac{1}{T_s} - \frac{1}{T_w}\right), \tag{50}$$

where $\Sigma = P dx$ being the area of surface element along the pipe wall. Substituting Eqs. (47)–(50) into Eq. (46), we obtain the total entropy generation in the volume element dV:

$$S_{\mathrm{gen}} = dx \int_{A_c} \frac{k}{T^2}\left(\frac{\partial T}{\partial r}\right)^2 dA + dx \int_{A_c} \frac{\mu}{T}\left(\frac{du}{dr}\right)^2 dA + P dx \frac{\mu}{\pi T_s} u_s \left(\frac{du}{dr}\right)_s + P dx q\left(\frac{1}{T_s} - \frac{1}{T_w}\right). \tag{51}$$

A dimensionless entropy generation number is introduced as:

$$\mathrm{N}_s = \frac{S_{\mathrm{gen}}}{\frac{k}{R^2} A_c dx} = \frac{S_{\mathrm{gen}}}{\pi k dx}. \tag{52}$$

Eq. (52) consists of two parts: $\mathrm{N}_s = \mathrm{N}_{s,\mathrm{b}} + \mathrm{N}_{s,\mathrm{i}}$, with bulk part $\mathrm{N}_{s,\mathrm{b}}$ representing the irreversibility induced by heat conduction and fluid flow, interfacial part $\mathrm{N}_{s,\mathrm{i}}$ the irreversibility induced by velocity slip and temperature jump. When $\mathrm{N}_{s,\mathrm{i}}$ is neglected, Eq. (52) reduces to the classical definition of entropy generation number in previous work [19]. $\mathrm{N}_{s,\mathrm{b}}$ is calculated through rectangular numerical integration by putting the velocity distribution Eq. (38) and temperature distribution Eq. (44) into Eq. (51), whereas $\mathrm{N}_{s,\mathrm{i}}$ is analytically obtained:

$$\mathrm{N}_{s,\mathrm{i}} = \mathrm{N}_{s,\mathrm{iT}} + \mathrm{N}_{s,\mathrm{iV}} = 2\left(\frac{1}{\theta_s} - \frac{1}{\theta_w}\right) + \frac{128 Kn}{(1 + 8Kn)^2} \frac{Br}{\pi \theta_s}. \tag{53}$$

3.2. Heat convection in micro-channel

The velocity distribution is obtained through a solution of Navier–Stokes equation with the first-order slip boundary condition Eq. (33) [4]:

$$u = \frac{3}{2} u_m \frac{1 + 4Kn - (y/H)^2}{1 + 6Kn}, \tag{54}$$

with the Knudsen number defined as $Kn = \lambda/2H$. The temperature differential equation in this case is [45]:

$$\rho c_p u \frac{\partial T}{\partial x} = k \frac{\partial^2 T}{\partial y^2} + \mu \left(\frac{du}{dy}\right)^2. \tag{55}$$

Through similar procedures in Section 3.1, the analytical solution of dimensionless temperature distribution is obtained:

$$\theta = \theta_w - \frac{4\gamma}{\gamma + 1} \frac{Kn}{\mathrm{Pr}} + \mathrm{B}_2(Y^2 - 1) + \mathrm{A}_2(1 - Y^4), \tag{56}$$

with the dimensionless temperature and coordinate respectively introduced as $\theta = kT/qH$, $Y = y/H$, and Brinkman number: $Br = \mu u_m^2 / 2Hq$. The combinational parameters A_2, B_2 are defined as:

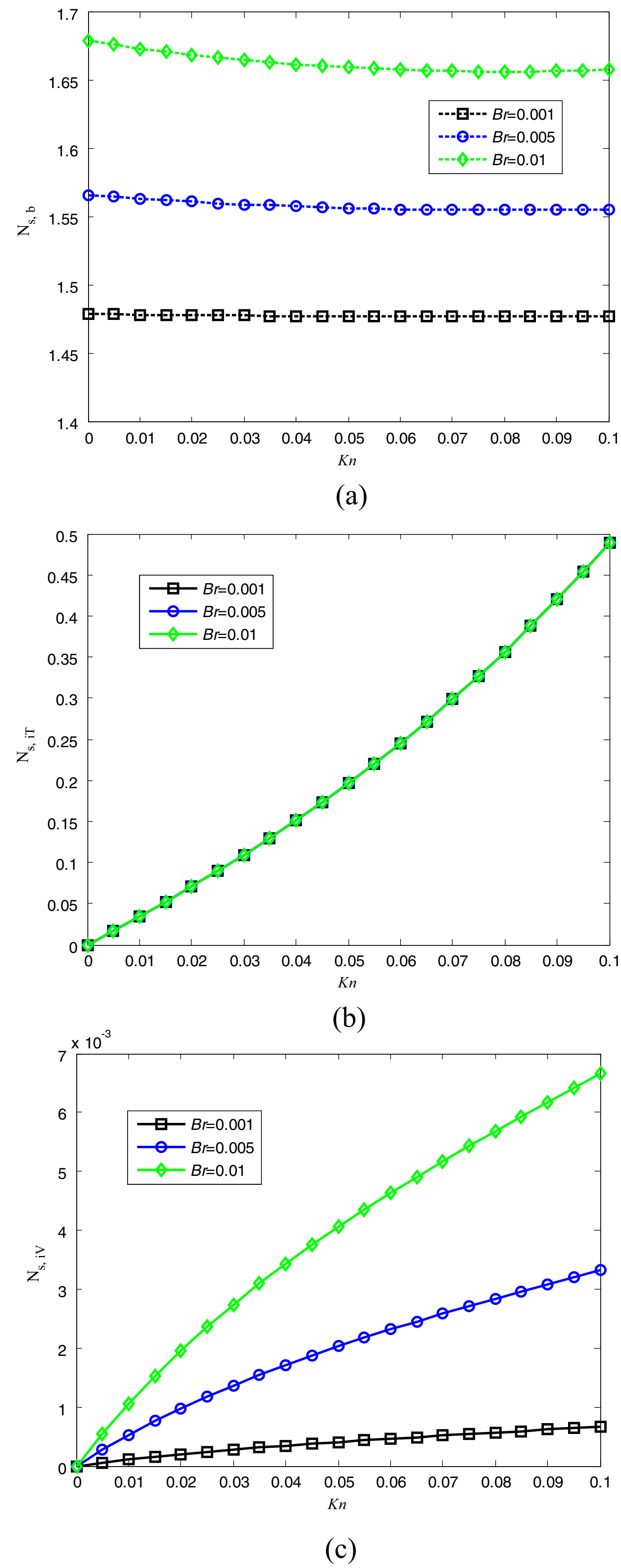

Fig. 6. Entropy generation number versus Kn for heat convection in micro-channel: (a) bulk entropy generation number; (b) interfacial entropy generation number induced by temperature jump; (c) interfacial entropy generation number induced by velocity slip. $\mathrm{Pr} = 0.71$, $\gamma = 1.4$, $\theta_w = 1$. Three different Brs are considered: $Br = 0.001$ (black square-line), $Br = 0.005$ (blue circle-line), $Br = 0.01$ (green diamond-line). The dashed lines with symbols represent the bulk entropy generation number whereas the solid lines with symbols represent the interfacial entropy generation numbers. (For interpretation of the references to color in this figure legend, the reader is referred to the web version of this article.)

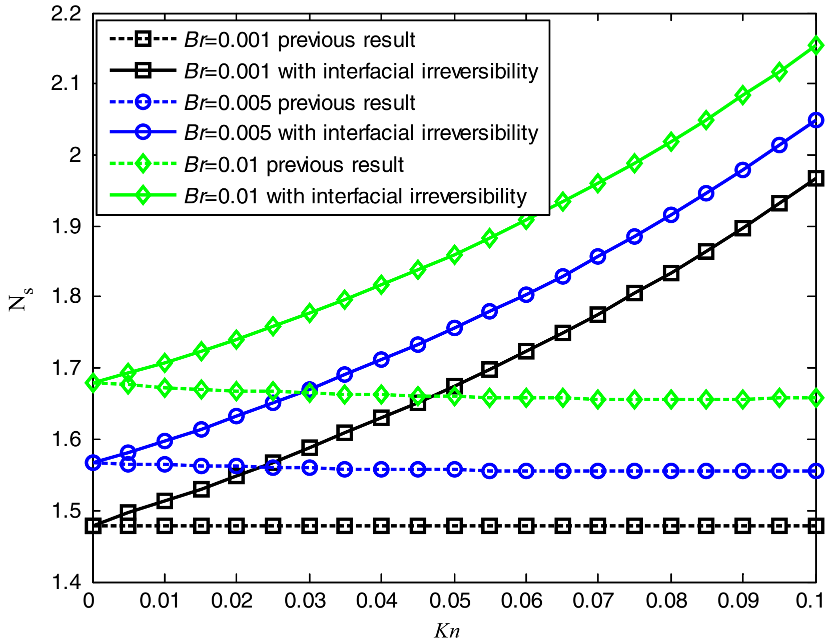

Fig. 7. Total entropy generation number of heat convection in micro-channel versus Kn. Pr = 0.71, γ = 1.4, θ_w = 1. Three different Brs are considered: Br = 0.001 (black square-line), Br = 0.005 (blue circle-line), Br = 0.01 (green diamond-line). The solid lines with symbols represent the present second-law analysis counting both the bulk and interfacial entropy generations, while the dashed lines with symbols represent the previous second-law analysis counting only the bulk entropy generation. (For interpretation of the references to color in this figure legend, the reader is referred to the web version of this article.)

$$\mathrm{A}_2 \equiv \left[1+\frac{18Br(1+4Kn)}{(1+6Kn)^2}\right]\frac{1}{8(1+6Kn)}$$
$$\mathrm{B}_2 \equiv \frac{3}{4}\left[1+\frac{6Br}{(1+6Kn)^2}\right]\frac{1+4Kn}{1+6Kn} \quad (57)$$

Again the velocity and temperature distribution solutions agree exactly with those in previous work [19,38], and are then used to calculate the entropy generation. Through similar procedures in Section 3.1, the total entropy generation and the entropy generation numbers of heat convection in micro-channel are obtained. The total entropy generation in the volume element $dV = A_c dx$ with unit width of channel ($P = 2$) is:

$$S_{gen} = dx\int_{A_c}\frac{k}{T^2}\left(\frac{\partial T}{\partial y}\right)^2 dA + dx\int_{A_c}\frac{\mu}{T}\left(\frac{du}{dy}\right)^2 dA + Pdx\frac{\mu}{\pi T_s}u_s\left(\frac{du}{dy}\right)_s + Pdxq\left(\frac{1}{T_s}-\frac{1}{T_w}\right). \quad (58)$$

The total entropy generation number is defined as: $\mathrm{N}_s = \frac{S_{gen}}{\frac{k}{H^2}A_c dx} = \frac{S_{gen}}{\frac{2k}{H}dx} = \mathrm{N}_{s,b} + \mathrm{N}_{s,i}$. The bulk part $\mathrm{N}_{s,b}$ is also computed through rectangular numerical integration by putting the velocity distribution Eq. (54) and temperature distribution Eq. (56) into Eq. (58). The interfacial part $\mathrm{N}_{s,i}$ is analytically obtained:

$$\mathrm{N}_{s,i} = \mathrm{N}_{s,iT} + \mathrm{N}_{s,iV} = \left(\frac{1}{\theta_s}-\frac{1}{\theta_w}\right) + \frac{36Kn}{(1+6Kn)^2}\frac{Br}{\pi\theta_s}. \quad (59)$$

4. Results and discussions

4.1. Heat convection in micro-pipe

The bulk entropy generation number, interfacial entropy generation numbers are plotted versus Knudsen number in Fig. 4(a), (b) and (c) respectively. The variation of total entropy generation number versus the Knudsen number is shown in Fig. 5. Three typical Brinkman numbers Br = 0.001, 0.005, 0.01 are compared.

4.2. Heat convection in micro-channel

The bulk and interfacial, and total entropy generation numbers versus Knudsen number at three different Brinkman numbers are shown in Figs. 6 and 7 respectively.

The results in Figs. 4(a) and 6(a) show that the bulk entropy generation in microscale heat convection decreases with increasing Kn, which may be explained by more flattened profiles and smaller gradients of velocity and temperature distributions. This trend is consistent with the commonly accepted knowledge in much previous work [18–28]. However, with increasing Kn, the interfacial entropy generation increases due to temperature jump and velocity slip, as shown in Figs. 4(b), (c) and 6(b), (c). The discontinuous temperature and velocity profiles represent the non-equilibrium effect at the gas–solid interface. Thus larger temperature jump and velocity slip at elevated Kn induce more irreversibility, resulting in more interfacial entropy generation. The increase of interfacial entropy generation dominates over the decrease of bulk entropy generation, giving rise to an increase of total entropy generation when Kn increases. This is a totally different trend from previous classical result as compared in Figs. 5 and 7, and indicates the dominance of interfacial irreversibility in microscale heat convection. The evaluation of thermodynamic performance of microscale system will be much distorted when the interfacial non-equilibrium effects are not taken into account. It is also seen that larger Br results in more bulk entropy generation, and more interfacial entropy generation caused by velocity slip; in contrast, the interfacial entropy generation caused by temperature jump is independent of Br. Overall, the total entropy generation increases with Br. In terms of the separate effect of temperature jump and velocity slip in the present cases, the former plays a main role and produces entropy generation about one order of magnitude larger than the latter. Nevertheless, the entropy generation caused by velocity slip will become larger at elevated *Br* as inferred from Eqs. (53) and (59).

5. Conclusions

The second-law analysis of microscale gas flow and heat transfer is investigated in a systematical way. The total entropy generation includes twofold: the bulk part from velocity and temperature gradients, and the interfacial part from velocity slip and temperature jump. The bulk and interfacial entropy generations are derived in the frame of classical irreversible thermodynamic and kinetic theory of gases respectively. The former part decreases with increasing *Kn*, as consistent with the conclusion in previous work. However, the latter part usually ignored in previous second-law analysis, is proportional to the magnitude of velocity slip and temperature jump, and increases with increasing *Kn*. The increase of interfacial entropy generation may dominate over the decrease of bulk entropy generation, leading to an increase of total entropy generation at elevated *Kn*. Our theoretical formalism is demonstrated by two classical cases of heat convection in micro-pipe and micro-channel within slip regime. The results infer that neglecting the interfacial irreversibility in evaluating the thermodynamic performance of microscale systems may lead to a contrary decision. The present work mainly aims at clarifying the physical nature and mathematical formulation of entropy generation in microscale heat and fluid flow. More work will be considered in the near future on more complicated situations, such as the isothermal boundary, axial heat conduction, other duct geometries and more realistic gas-surface interactions beyond the fully diffuse walls.

Acknowledgements

This work is financially supported by the Key Basic Scientific Research Program (2013CB228301) and the Tsinghua University Initiative Scientific Research Program.

References

[1] H.S. Nalwa, Encyclopedia of Nanoscience and Nanotechnology, American Scientific Publishers, California, 2004.
[2] M. Gad-el-Hak, The MEMS Handbook: MEMS Introduction and Fundamentals, Taylor & Francis, New York, 2006.
[3] M. Wang, Z. Li, Nonideal gas flow and heat transfer in micro- and nanochannels using the direct simulation Monte Carlo method, Phys. Rev. E 68 (4) (2003) 46704.
[4] G. Karniadakis, A. Beskok, N. Aluru, Microflows and Nanoflows: Fundamentals and Simulation, Springer, New York, 2005.
[5] M. Wang, X.D. Lan, Z.X. Li, Analyses of gas flows in micro- and nanochannels, Int. J. Heat Mass Transfer 51 (13–14) (2008) 3630–3641.
[6] G.A. Radtke, N.G. Hadjiconstantinou, Variance-reduced particle simulation of the Boltzmann transport equation in the relaxation-time approximation, Phys. Rev. E 79 (5) (2009) 056711.
[7] F. Sharipov, Rarefied Gas Dynamics: Fundamentals for Research and Practice, Wiley-VCH, Weinheim, 2016.
[8] G. Chen, Nanoscale Energy Transport and Conversion: a Parallel Treatment of Electrons, Molecules, Phonons, and Photons, Oxford University Press, New York, 2005.
[9] D. Jou, J. Casas-Vázquez, G. Lebon, Extended Irreversible Thermodynamics, Springer, Heidelberg, 2010.
[10] Y. Guo, M. Wang, Phonon hydrodynamics and its applications in nanoscale heat transport, Phys. Rep. 595 (2015) 1–44.
[11] F. Sharipov, Heat transfer in the Knudsen layer, Phys. Rev. E 69 (6) (2004) 061201.
[12] V.A. Cimmelli, A. Sellitto, D. Jou, Nonequilibrium temperatures, heat waves, and nonlinear heat transport equations, Phys. Rev. B 81 (5) (2010) 054301.
[13] D. Jou, G. Lebon, M. Criado-Sancho, Variational principles for thermal transport in nanosystems with heat slip flow, Phys. Rev. E 82 (3) (2010) 031128.
[14] F. Vázquez, J. del Rio, Thermodynamic characterization of the diffusive transport to wave propagation transition in heat conducting thin films, J. Appl. Phys. 112 (12) (2012) 123707.
[15] A. Bejan, A study of entropy generation in fundamental convective heat transfer, J. Heat Transfer 101 (11) (1979) 718–725.
[16] H. Herwig, The role of entropy generation in momentum and heat transfer, J. Heat Transfer 134 (3) (2012) 031003.
[17] S.R. De Groot, P. Mazur, Non-equilibrium Thermodynamics, Dover Publications, New York, 1962.
[18] M. Avci, O. Aydin, Second-law analysis of heat and fluid flow in microscale geometries, Int. J. Exergy 4 (3) (2007) 286–301.
[19] K. Hooman, Entropy generation for microscale forced convection: Effects of different thermal boundary conditions, velocity slip, temperature jump viscous dissipation, and duct geometry, Int. Commun. Heat Mass Transfer 34 (8) (2007) 945–957.
[20] A. Arikoglu, I. Ozkol, G. Komurgoz, Effect of slip on entropy generation in a single rotating disk in MHD flow, Appl. Energy 85 (12) (2008) 1225–1236.
[21] M. Yari, Entropy generation analysis for Couette–Poiseuille flow through parallel-plates microchannel, Int. J. Exergy 6 (6) (2009) 809–825.
[22] A. Sadeghi, M.H. Saidi, Second law analysis of slip flow forced convection through a parallel plate microchannel, Nanoscale Microscale Thermophys. Eng. 14 (4) (2010) 209–228.
[23] G. Ibanez, A. Lopez, J. Pantoja, J. Moreira, J.A. Reyes, Optimum slip flow based on the minimization of entropy generation in parallel plate microchannels, Energy 50 (2013) 143–149.
[24] M. Shojaeian, A. Kosar, Convective heat transfer and entropy generation analysis on Newtonian and non-Newtonian fluid flows between parallel-plates under slip boundary conditions, Int. J. Heat Mass Transfer 70 (2014) 664–673.
[25] E. Ogedengbe, G. Naterer, M. Rosen, Slip-flow irreversibility of dissipative kinetic and internal energy exchange in microchannels, J. Micromech. Microeng. 16 (10) (2006) 2167–2176.
[26] K. Hooman, Heat transfer and entropy generation for forced convection through a microduct of rectangular cross-section: Effects of velocity slip, temperature jump, and duct geometry, Int. Commun. Heat Mass Transfer 35 (9) (2008) 1065–1068.
[27] S. Chen, Z. Tian, Entropy generation analysis of thermal micro-Couette flows in slip regime, Int. J. Therm. Sci. 49 (11) (2010) 2211–2221.
[28] L. Kuddusi, First and second law analysis of fully developed gaseous slip flow in trapezoidal silicon microchannels considering viscous dissipation effect, Int. J. Heat Mass Transfer 54 (1–3) (2011) 52–64.
[29] F. Sharipov, Onsager–Casimir reciprocity relations for open gaseous systems at arbitrary rarefaction: I. General theory for single gas, Phys. A: Stat. Mech. App. 203 (3) (1994) 437–456.
[30] L. Waldmann, Non-equilibrium thermodynamics of boundary conditions, Z. Naturforsch. A 22 (8) (1967) 1269–1280.
[31] D. Bedeaux, A. Albano, P. Mazur, Boundary conditions and non-equilibrium thermodynamics, Physica A 82 (3) (1976) 438–462.
[32] H. Vestner, L. Waldmann, Boundary conditions for the distribution function and for the moments of a gas at a moving wall, Z. Naturforsch. A 34 (3) (1979) 269–283.
[33] V. Roldughin, Non-equilibrium thermodynamics of boundary conditions for slightly rarefied gases, J. Non-Equilib. Thermodyn. 16 (1) (1991) 13–26.
[34] V.M. Zhdanov, V.I. Roldugin, Non-equilibrium thermodynamics and kinetic theory of rarefied gases, Phys. Usp. 41 (4) (1998) 349–378.
[35] F. Sharipov, Onsager–Casimir reciprocity relations for open gaseous systems at arbitrary rarefraction: II. Application of the theory for single gas, Phys. A: Stat. Mech. App. 203 (3) (1994) 457–485.
[36] F. Sharipov, Onsager–Casimir reciprocal relations based on the Boltzmann equation and gas-surface interaction: Single gas, Phys. Rev. E 73 (2) (2006) 026110.
[37] O. Aydin, M. Avci, Heat and fluid flow characteristics of gases in micropipes, Int. J. Heat Mass Transfer 49 (9–10) (2006) 1723–1730.
[38] O. Aydin, M. Avci, Analysis of laminar heat transfer in micro-Poiseuille flow, Int. J. Therm. Sci. 46 (1) (2007) 30–37.
[39] L.D. Landau, E.M. Lifshitz, Fluid Mechanics, Elsevier Pte Ltd., Singapore, 2004.
[40] S. Chapman, T.G. Cowling, The Mathematical Theory of Non-uniform Gases, Cambridge University Press, Cambridge, 1953.
[41] P.L. Bhatnagar, E.P. Gross, M. Krook, A model for collision processes in gases. I. small amplitude in charged and neutral one-component systems, Phys. Rev. 94 (3) (1954) 511–525.
[42] H. Struchtrup, Macroscopic Transport Equations for Rarefied Gas Flows, Springer-Verlag, Heidelberg, 2005.
[43] G.M. Kremer, An Introduction to the Boltzmann Equation and Transport Processes in Gases, Springer, Heidelberg, 2010.
[44] C. Cercignani, The Boltzmann Equation and its Applications, Springer, New York, 1988.
[45] T. Bergman, A. Lavine, F. Incorpera, D. DeWitt, Fundamentals of Heat and Mass Transfer, John Wiley & Sons Inc, Hoboken, 2011.